TWELFTH EUROPEAN ROTORCRAFT FORUM

Paper N° 40

AN ANALYSIS OF IN-FIN TAIL ROTOR NOISE

M. Roger and F. Fournier

Ecole Centrale de Lyon - Centre Acoustique

Ecully, France

September 22 - 25, 1986

Garmisch-Partenkirchen

Federal Republic of Germany

Deutsche Gesellschaft für Luft- und Raumfahrt e. V. (DGLR)

Godesberger Allee 70, D-5300 Bonn 2, F.R.G.

ABSTRACT

This paper is concerned with some aspects of the sound generation and sound propagation from a fenestron in-fin tail rotor.

The study includes the three following parts :

- a prediction of rotor-noise sources using calculations based on unsteady aerodynamics theory,
- an experimental investigation of the diffraction caused by the casing,
- the definition of an acoustic testing procedure on a real complete version of a fenestron-type tail rotor.

Each part was performed independently. All the results given here are therefore only preliminary results, which must be considered as a first attempt towards the understanding of the noise generated by an in-fin tail rotor.

1. INTRODUCTION

The various sources of aerodynamically generated noise on helicopters are principally associated with the two rotors, namely the main rotor and the tail rotor. In the case where the latter is an in-fin one, the basic frequencies emitted (related to the speed of rotation and the number of blades) are higher than those radiated by the former. As a consequence a specific study of tail rotors is essential.

Actually, the in-fin tail rotor is more like a stage of an axial turbomachine. Indeed it is composed of a rotor and outlet guide vanes placed in a short casing. Consequently, a study of the emitted noise in such a configuration is doubly complicated :

- the flow around and through a tail rotor is generally highly disturbed,
- the casing is too short for the well-known cut-off effect on acoustic modes in a duct to occur. Accordingly it acts somewhat as a scattering body.

The purpose of the paper is to tackle the problem, focusing on three complementary aspects :

. Firstly, an original acoustic equipment added to the fenestron test rig at Aérospatiale-Marignane is described. The results of this section are twofold : on one hand they provide spectra and directivity diagrams that can be compared to the results of the two following sections. On the other hand, they permit to bring out the full set of characteristics of a given rotor-stator configuration.

. Secondly, using an unsteady aerodynamics code, a computation of the noise generated by the rotor in a disturbed flow is performed, in order to show the influence of parameters such as the forward flight speed, the pitch angle of the blades, the anisotropy of the umpstream turbulence, etc... ; it permits to know whether the noise generated is broadband or more specially concentrated at blade passing frequencies (BPF tones). The presence of a casing is not taken into account.

. Finally, the diffraction due to the casing is experimentally determined by means of a half-scaled model set up in the anechoic room of the Ecole Centrale de Lyon. Flow effects on sound propagation are deliberately ignored and real sources are replaced by a spinning modes simulator.

For the moment this part of the study is appropriate for noise spectra dominated by BPF tones. The simulator is composed of a crown of very small mutually out-of-phase loudspeakers, each of which receives the frequency relating to the desired mode.

2. ACOUSTIC EQUIPMENT AND MEASUREMENTS

The experimental set up used on the Marignane test rig is schematically shown in fig. n° 1. The basic facility consists of a full-scale fenestron without drift, the rotor of which, blowing upward, lies in a horizontal plane 2.75 m. above of the ground.

Acoustic measurements had to be performed in a vertical half-plane containing the rotor axis and corresponding to a domain below the trim-plane for an actual helicopter in forward flight. For these reasons a vertically curved rail was constructed, using an I-shaped iron. A moving carriage with two B.K. 1/4-inch microphones is then installed on the rail and can be driven by remote control.

The curvature radius of the rail is 2.4 m, and it covers a 126° angular range. Stoppings at the 22 provided measuring stations automatically result, as small on-the-rail pins intercept the pencil of a photocell attached to the carriage.No attempt was made in the immediate vicinity of the blowing zone, in order to prevent mechanical damage and avoid measuring non-acoustic disturbances.

Results

Measurements were made for two rotor versions and several values of the mean blade pitch angle, namely -8°, 0°, 8°, 16°, 32°, 40°. Results consist of narrow-band analysis spectra in the range 0-10 kHz and directivity diagrams interpolated from the 22 measuring-stations. Examples are given in figures n° 2, 3, 4.

Generally speaking, noise spectra exhibit a well-defined structure of sharp peaks corresponding to blade passing frequency and harmonics (BPF tones family).

Nevertheless an exception occurs in the case of zero mean pitch angle. Then BPF tones rapidly disappear (only the first two are still discernible) and are replaced by another family of slightly wider "haystacks" centered on different frequencies. This phenomenon could be due to the fact that the mean outflow vanishes. Some recirculations are then possible in the rotor vicinity, resulting in a preliminary rotation at the inlet. This point will be discussed in the following section.

The OASPL directivity patterns are shown in fig. 4 for the two versions, and two values of the blade pitch angle. The radiated noise is practically nondirectional, except near the rotor axis and near the rotor plane, where a slight attenuation is noticed.

As we shall see in section 4, the on-axis minimum is the contribution of a spinning modes behavior associated with BPF tones. The rotor plane minimum is a possible consequence of both natural directivity of rotor noise sources and a masking effect due to the casing.

Finally, measurements permitted to compare the characteristics of the two tested rotors. Figure n° 5 shows, for several values of pitch angle, a relative OASPL criterion. Version 1 appears to be the most satisfactory one, from the acoustic point of view. The lowest noise level occurs for a pitch angle of 8°.

3. AEROACOUSTICS CALCULATIONS

Rotor noise mechanisms

Helicopters generally operate in different flight configurations, each of which corresponds to specified values of the pitch angle of the rotor blades and to various inflow conditions. Accordingly a typical tail rotor noise spectrum can have a changing behavior.

During static hovering, for example, the pitch angle reaches high values and the rotor operates in a full suction condition. Mean streamlines are then convergent, so that atmospheric turbulent eddies can be strongly elongated, acquiring high anisotropy levels. In such an inflow configuration they become very coherent with respect to the rotor, and as a result produce a true peak noise at the BPF tones ([1]).

In the case of the static test, which is involved here, an additional source of this type of coherent noise is the existence of ground vortices, and possible phenomena related to recirculating flows.

Conversely, when no significant contraction of the mean flow occurs, as is the case in forward flight with zero pitch angle, turbulent eddies are responsible for true random disturbances on the disk of the rotor, so that a wide-band noise is emitted.

Other kinds of aerodynamical disturbances also arise in flight, such as flap wakes, turbulent boundary layers, gas-turbine exhaust flows, and tip vortices generated by the main-rotor blades.

In-flight configuration

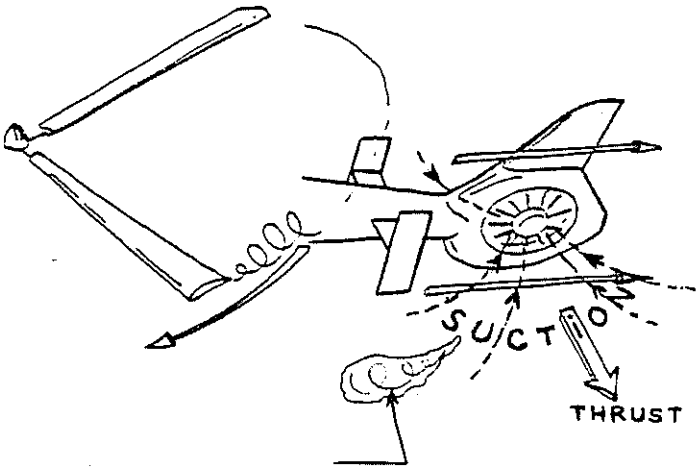

Contraction of turbulent eddies

Static test

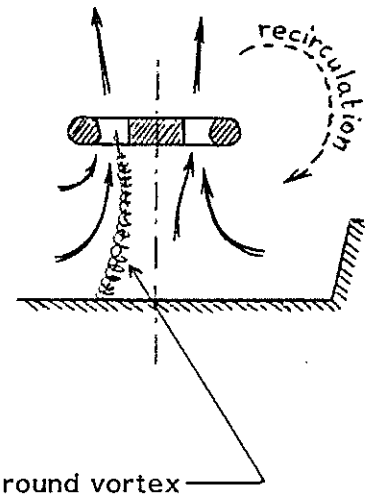

Ground vortex

The method used here to predict the rotor noise due to a turbulent inflow is based on the unsteady aerodynamics theory of isolated thin airfoils. Consequently steady loadings on blades are not taken into account (their contribution to radiated noise is negligible in comparison with unsteady ones).

This theoretical background is then extended to the case of a rotor by introducing a Doppler shift and a blade-to-blade correlation, following Amiet and Paterson (|2|). Details are given in ref. |3|. The main features of the code are the following :

- the acoustic frequencies are much higher than the rotational frequency ; this assumption is satisfied in the tail-rotor case,
- a two-dimensional compressible aerodynamic transfer function is used (|4|),
- the anisotropy of the inflow turbulence is described by an artificial elongation coefficient in the turbulence spectrum (Von Kármán reference spectrum).

Rotor noise results

Some of the numerical results are given in fig. n° 6 and compared to the measured spectrum (fig. n° 3).

This part of the study being only in its preliminary stage, no effort was made to obtain a perfect fitting. Nevertheless the graphs show that increasing anisotropy makes BPF emission stonger and narrower. A 20 % turbulent intensity and an anisotropy ratio of 40 (longitudinal scales 40 times transversal scales) would be necessary to explain the measured spectra by an inflow-rotor interaction mechanism. Such an anisotropy is perhaps possible with strong ground vortices and recirculating flows, but no experimental evidence of this has been obtained yet.

It is noticeable, that the qualitative behavior of rotor noise as calculated is reminiscent of the zero pitch angle spectrum of fig. n° 2. This could be an indication for a true rotor-noise mechanism, but with a lower rotation speed due to a preliminary intake rotation.

The stator problem

Another efficient source mechanism occurs when stator blades are swept by the wakes of the rotor blades. On one hand, a 20 % turbulence level is a possible value in this case ; on the other hand, the periodic part of the velocity defect in the wakes acts as a very coherent disturbance. Then the rotor-stator interaction mechanism can be responsible for both wide-band level and sharp peak noise (see fig. n° 3).

It is worth noting that Hanson's method for the prediction of stator noise (|5|) was used (see fig. n° 7). Although a good agreement can be obtained, the selection of the two main parameters (the standard deviation of both phase and amplitude modulations of the velocity distribution in the rotor wakes) seems to be arbitrary.

To sum up at this point, the observed spectra on the Marignane test rig may have a two-sided origin. Be that as it may, truely random aerodynamic disturbances on the blades of the rotor and the stator can only produce wide-bande noise. BPF tones are due to periodic interactions. By performing a Fourier series analysis, the corresponding source waves can be described using the so-called spinning modes defined by Tyler and Sofrin (|6|). The propagation of such noise components is the matter of the following section.

4. DETERMINATION OF THE SCATTERING OF SPINNING MODES BY THE CASING

Simulation process

A given spinning mode is a periodic azimuthal structure characterized by three parameters :

- the radius R,
- an azimuthal wave-number n defining the angular periodicity $2\pi/n$ of the structure,
- the equivalent frequency ω in a fixed frame, related to n and to the rotation speed of the mode $\Omega = \omega/n$.

The associated pressure source distribution can be written :

$P_S(\alpha, t) \sim \cos(\omega t + n\alpha)$, α been defined below.

Practically, the modal composition of a single peak frequency emitted by a rotor-stator stage is too complicated for such a mode (R, n, ω)to be isolated. The only mean of studying it separately is then to have recourse to a spinning modes simulator.

The principle is as follows : it is possible to build up the acoustic field, which would be generated by the complete continuous mode, by a sampling of the source ; the mode is replaced by a circular array of m point sources, each of which operates at the frequency ω , and exhibits a $2\pi n/m$ phase shift with its immediate neighbor, in order to simulate rotation.

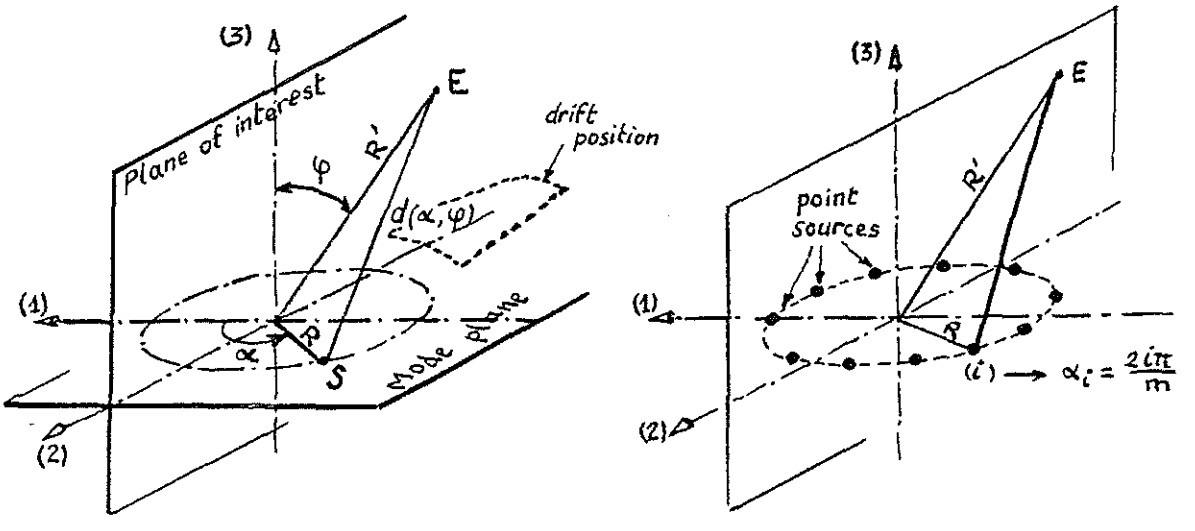

The pressure fluctuation at point E of the figure for the continuous mode is :

$$(1) \qquad P_E(\varphi, t) \sim \int_0^{2\pi} \cos\left\{\omega\left(t - \frac{d(\alpha,\varphi)}{c_0}\right) + n\alpha\right\} \frac{d\alpha}{d(\alpha,\varphi)}$$

It corresponds to a directivity diagram within the plane of interest, which is symmetric with respect to both axes (2) and (3). Moreover, no noise is radiated along the mode axis (3).

The resulting field generated by the simulated mode is :

$$(2) \qquad p'_E(\varphi,t) \sim \sum_{i=1}^{m} \frac{\cos\left\{\omega\left(t - \frac{d(\frac{2i\pi}{m},\varphi)}{c_o}\right) + \frac{2in\pi}{m}\right\}}{d\left(\frac{2i\pi}{m},\varphi\right)}$$

The above properties still hold, except for the symmetry with respect to axis (3), which is obtained only if m is an even number.

Obviously, it is also necessary to avoid undersampling, so that the simulation of a spinning mode with wavenumber n requires a number m at least equal to 2n.

Design of the simulator

In the present study, the spinning modes associated with BPF tones can arise from two general mechanisms :

- Steady aerodynamic loadings on rotor blades generate direct modes with an azimuthal wave-number n equal to a multiple of the number of blades B = 11. These modes have the same rotation speed as the rotor.
- Periodic inflow-rotor interactions and rotor-stator interactions generate so-called interaction modes, with a wave-number n given by $NB \pm kV$, V being the number of blades (V = 12) of the stator or the periodicity of the inflow distorsion.

Sources of the second kind are known to be the most efficient, very often with small values of n and various rotation speeds. This justifies the small number m of point sources used here for the simulation.

The technology employed for the simulator of the spinning modes is not a new topic ([7]). More precisely, the main purpose of the study was to build a compact, light and cheap simulator, easy to fit on a half-scaled model of a fenestron-type casing, so that directivity measurements could be performed in an anechoic room.

The emitting antenna is an array of 11 small diameter loudspeakers ($\phi \sim 1$ cm), movable along radially disposed rods. It is driven by a microprocessors system.

The assemblage of the antenna and the wooden model is shown in fig. n° 12. All measurements were made in the ECL anechoic-room at a distance of 5 meters from the center of the antenna, within the frequency range 800 - 5 000 Hz, and for various radial positions between the boundaries of the casing.

Results

Preliminary control tests relating to the free-field behavior of the simulator are summarized in figures 8 and 9.

Fig. n° 8 compares the theoretical directivity diagram of a continuous mode to that of the corresponding simulated mode by means of a perfect 11 sources simulator ; these calculations correspond respectively to equations (1) and (2). The expected discrepancy due to the undersampling for the n = 6 mode is noticed.

Nevertheless, by adjusting the source positions according to equation (2), it is possible to obtain a correct simulation in a validity domain covering the half-plane of interest. The 6-mode appears then to be the theoretical limit of the simulator.

Furthermore, Fig. 9 compares the perfect simulator results with the behavior of the real antenna. Other discrepancies occur, as a consequence of the size of the loudspeakers and of electronical connections.

Finally, the diffraction caused by the casing is shown in Fig. 10. Far-field directivity diagrams of the antenna in both free-field conditions and in-model conditions are superimposed. Two conclusions follow :

- the casing does not affect significantly the emission in directions close to the antenna axis,
- the directivity diagram is strongly modified in directions close to the antenna plane ; this appears to be due to the casing acting as a scattering body.

In the mean, it is then possible to define a so-called masking effect, which is responsible for the attenuation in directions close to the antenna plane. This effect is qualitatively represented in Fig. 11, where the difference between the directivity diagrams obtained respectively in free field conditions or with the model is considered.

CONCLUSIONS

In the present study, the problem of the noise generated by a fenestron tail-rotor was handled, following three complementary points of view.

At first, a simple procedure for acoustic measurements on a test rig provided for aerodynamic studies has been set up. This furnished very clear and usefull results, permitting an easy acoustic diagnosis.

A method of prediction of the rotor noise in a turbulent flow has also been defined, leading to a parametric study based on some determinant quantities, such as the rate of anisotropy of the inflow turbulence.

It follows that the sharp BPF structure of the experimentally observed spectra could be explained by a contraction of the atmospheric turbulence and by ground vortices, but could also result from a rotor-stator interaction. An answer to this question requires the continuation of the study towards the following points :

. the best possible knowledge of the inflow parameters during static tests,

. a prediction of the stator noise adapted to the fenestron.

Finally, the construction of a spinning modes simulator appeared to be the most powerfull mean of defining the masking effet caused by the fenestron on the BPF tones radiation. The first results here exhibit a significant attenuation (up to 10 dB) in directions close to the plane of the simulated rotor.

The next step will be to join the acquisitions of the two preceeding points to consistant values of the required parameters ; this will lead to a better understanding of the fenestron noise.

AKNOWLEDGMENTS

The authors wish to thank the Aérospatiale acousticians team and test rig team for their collaboration.

This work was supported by the Direction des Recherches Etudes et Techniques (DRET/METRAFLU n° 83.025 - 84.368).

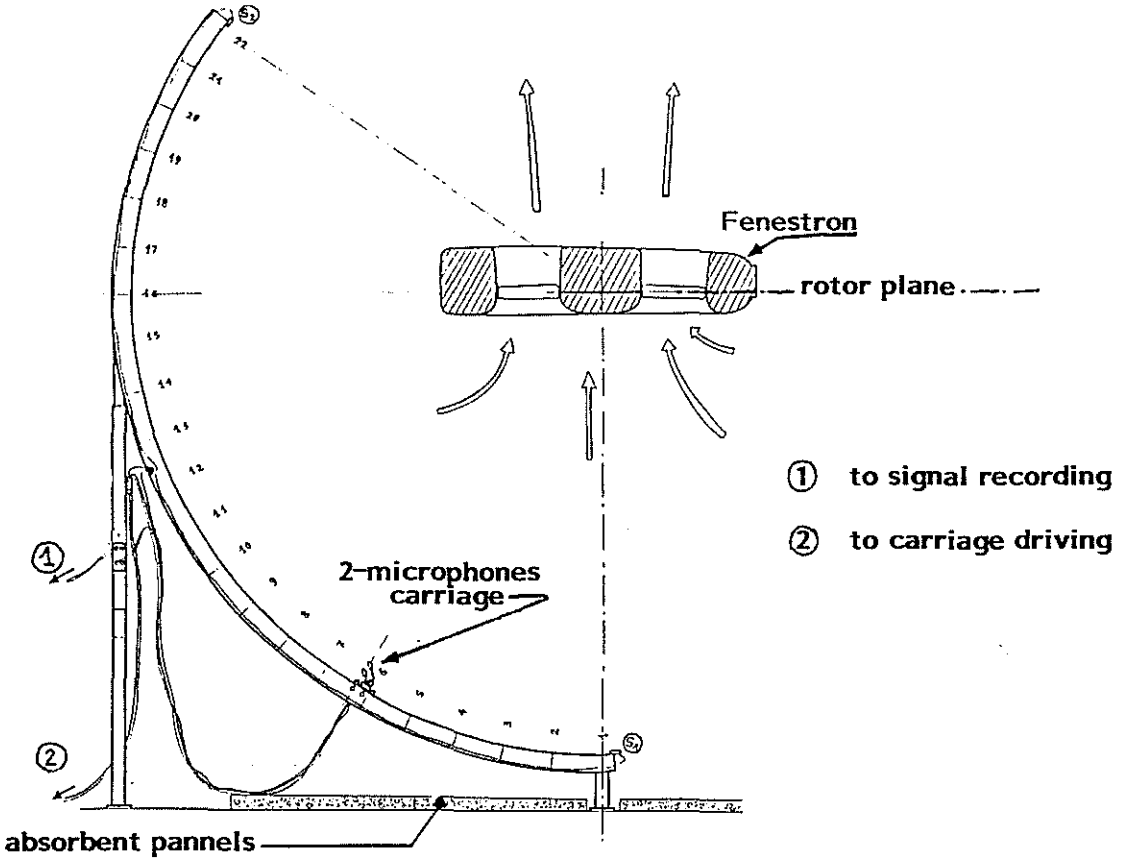

Fig. 1 - Acoustic installation for fenestron noise measurements.

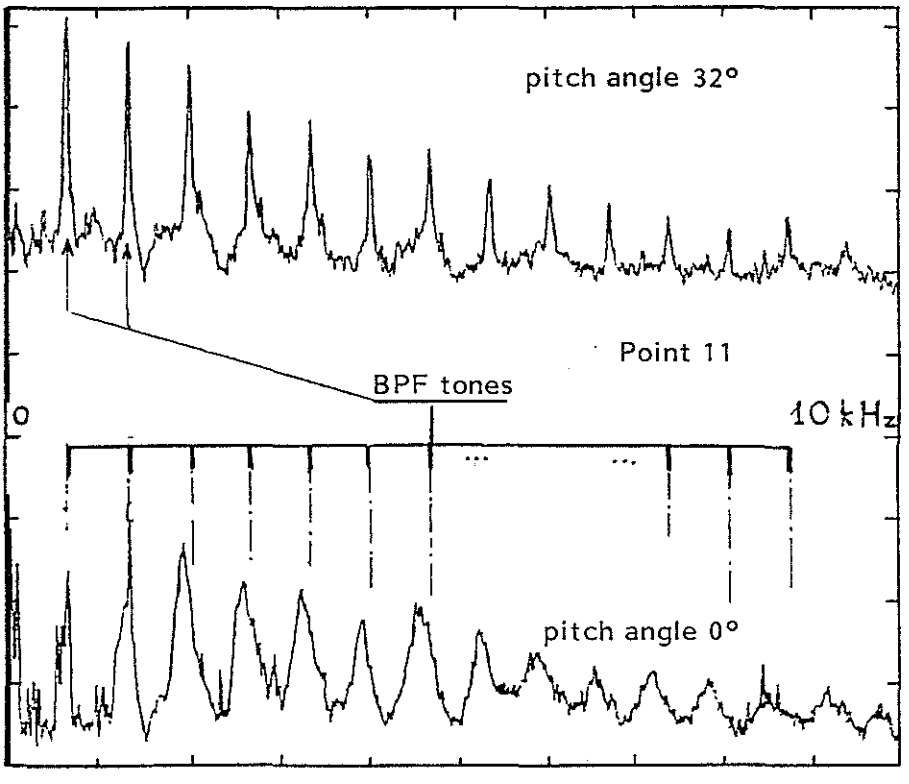

Fig. 2 - Measured noise spectra. Version n° 1 3 660 rpm.

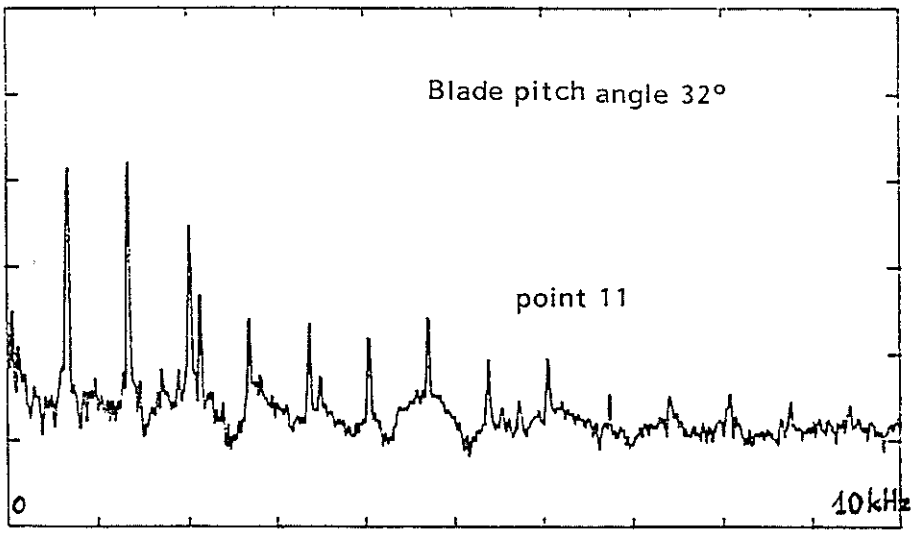

Fig. 3 - Measured noise spectrum Version 2.

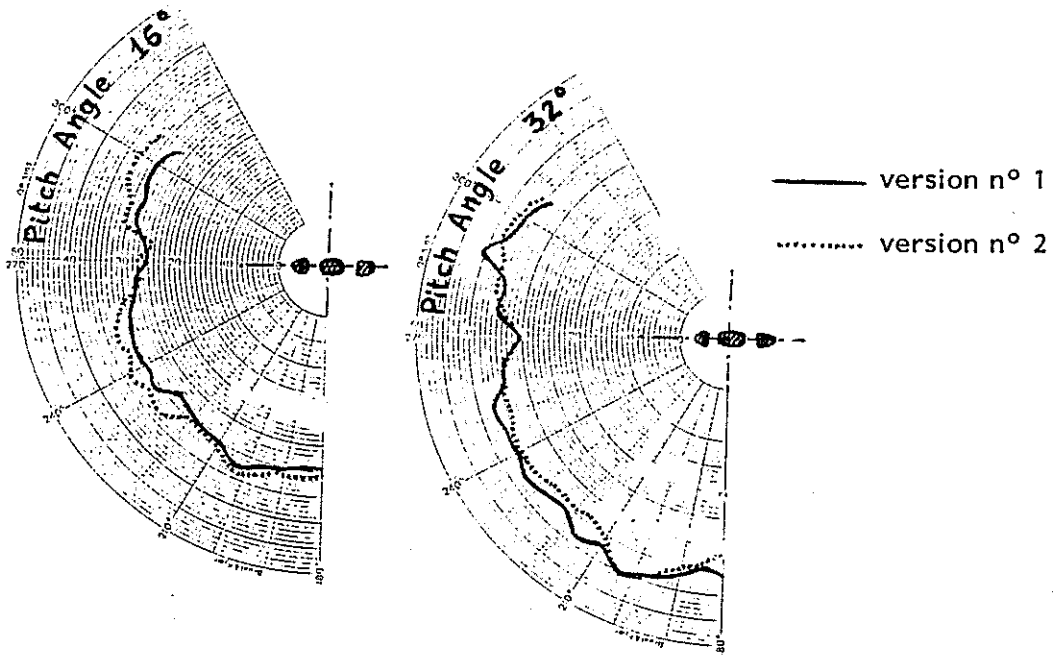

Fig. 4 - OASPL directivity measured on Marignane test rig.

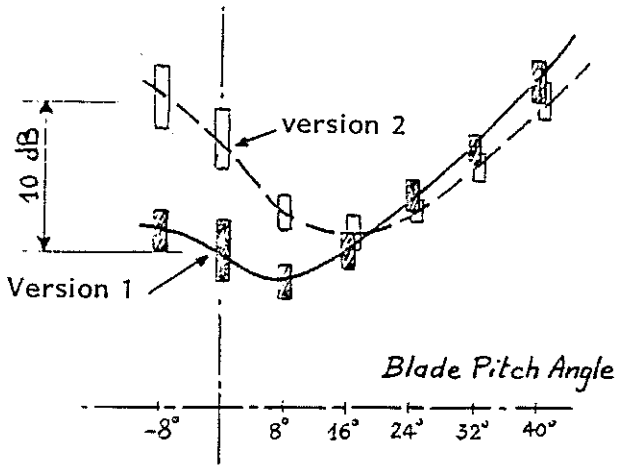

Fig. 5 - Comparison of OASPL performances versus pitch angle, for the two tested rotor versions.

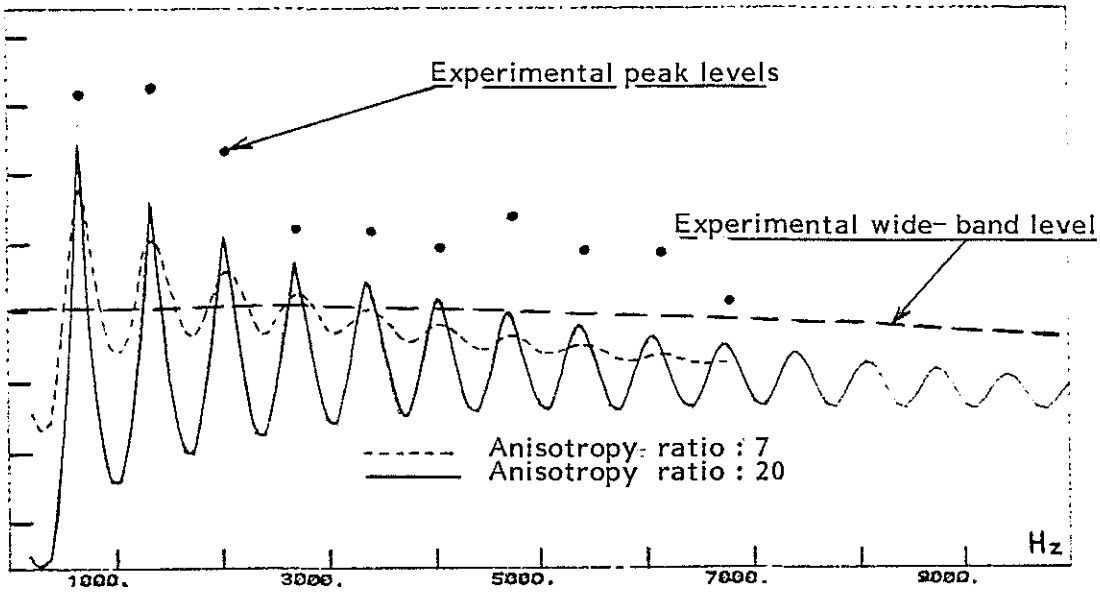

Fig. 6 - Rotor noise calculations (réf. n° 3)

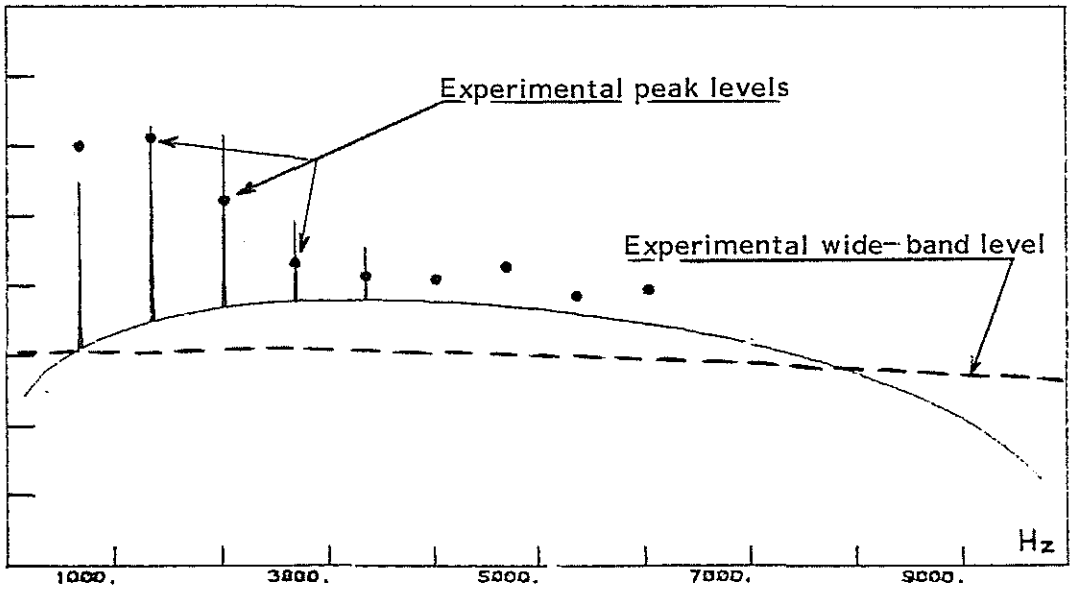

Fig. 7 - Stator noise calculations using Hanson's method.
Standard deviations :
phase 11 $\sigma_p = 0.065$
amplitude $\sigma_{am}/_{am} = 1.$

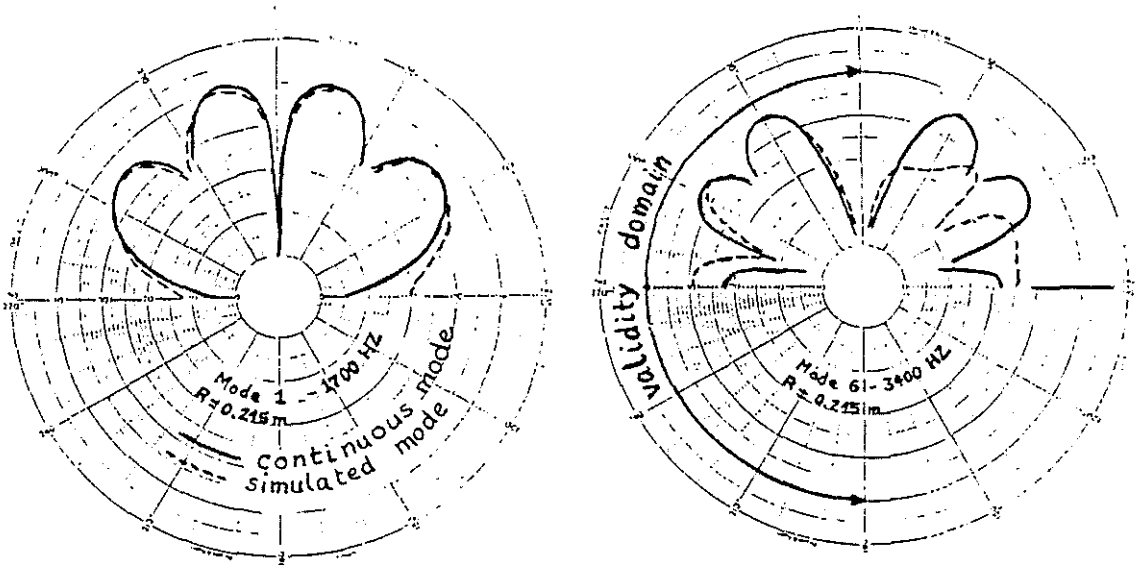

Fig. 8 - Validation of the simulation process.

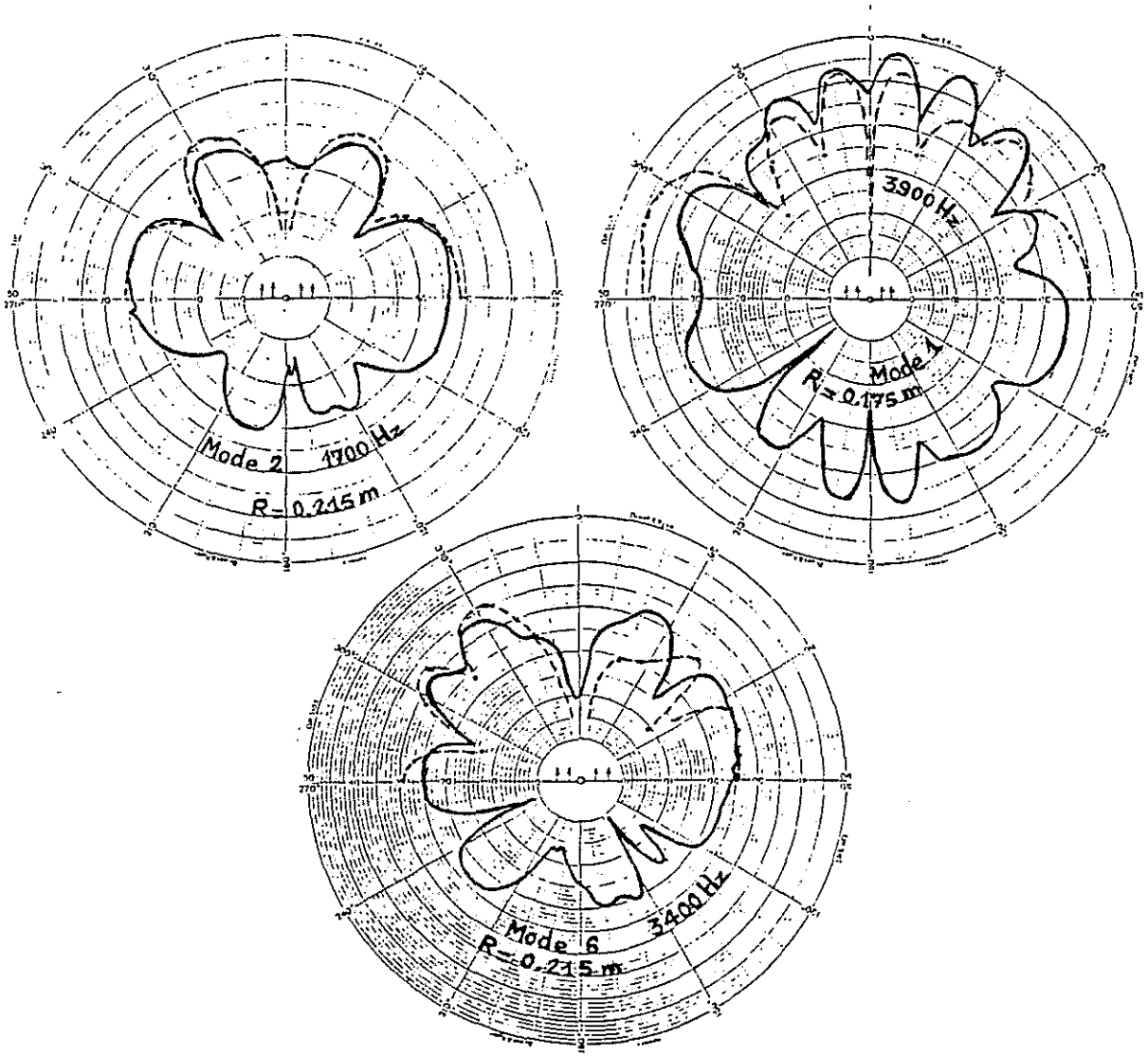

Fig. 9 - Validation test of the free-field antenna :
——— measured directivity at 5 m.
– – – – – theoretical directivity for a perfect simulated mode with 11 point sources.

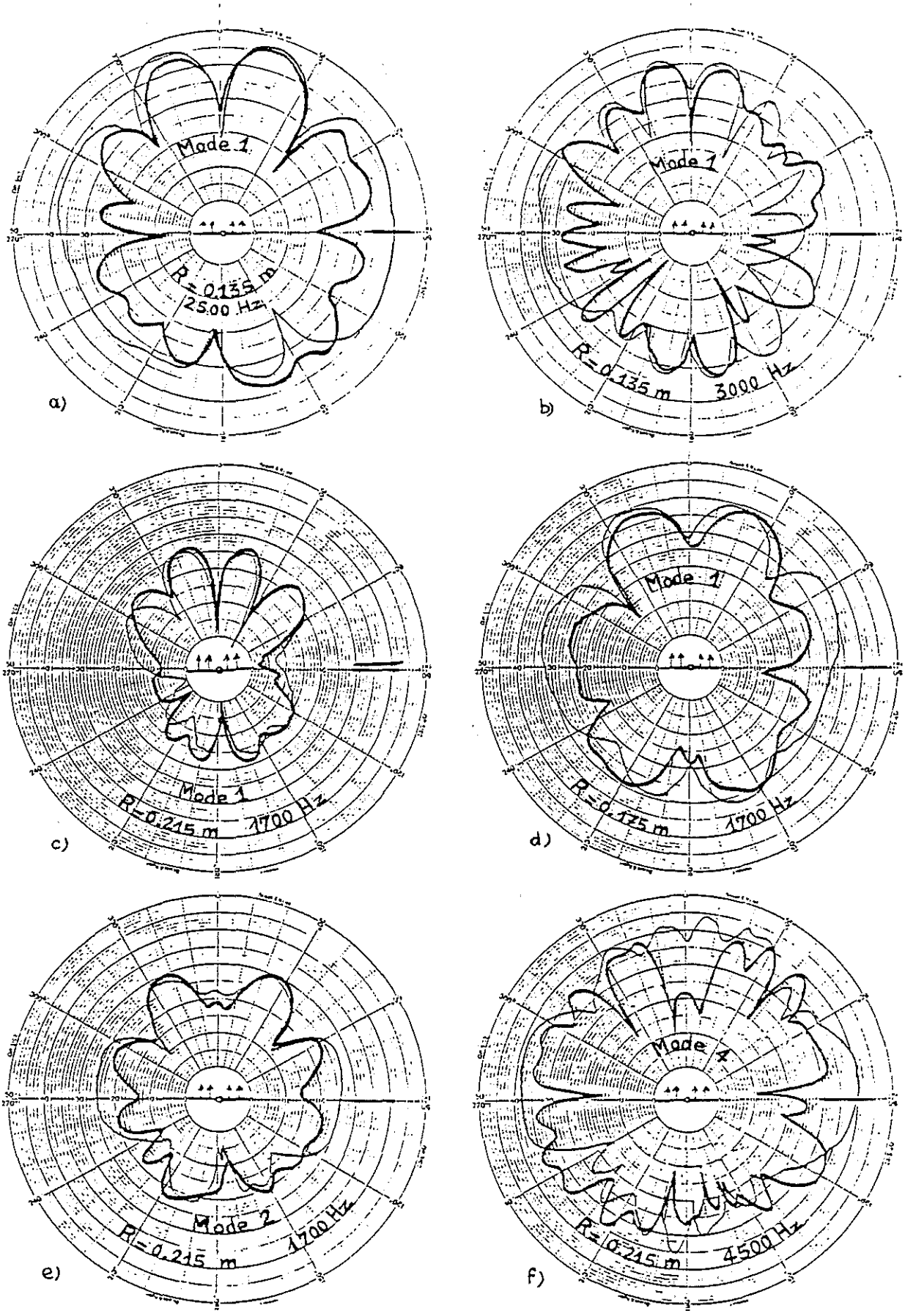

Fig. 10 - Diffraction due to the casing on several simulated spinning modes :
——— antenna-in-model directivity.
——— free-field directivity.

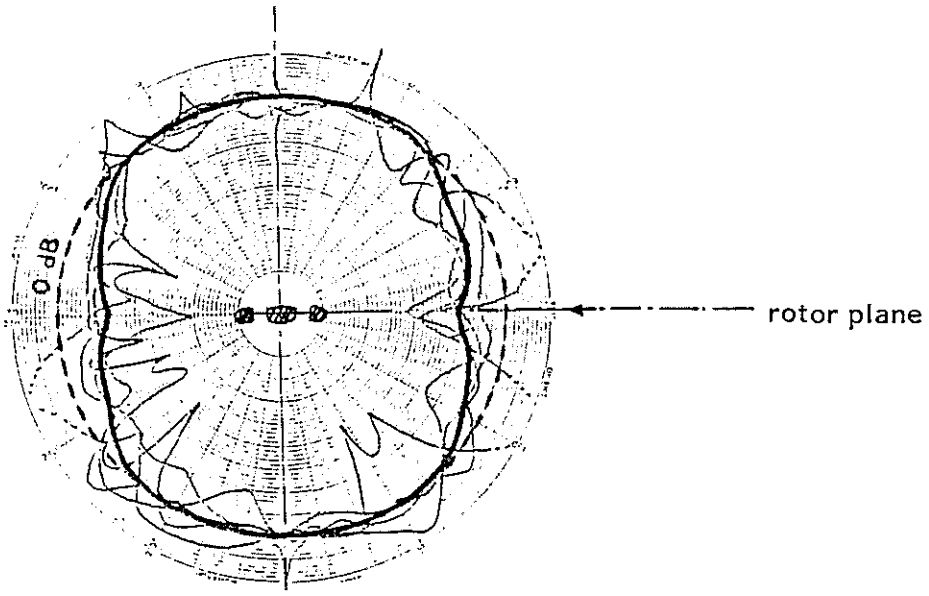

Fig. 11 - So-called masking effect (mean qualitative diffraction, based on some results from Fig.10).

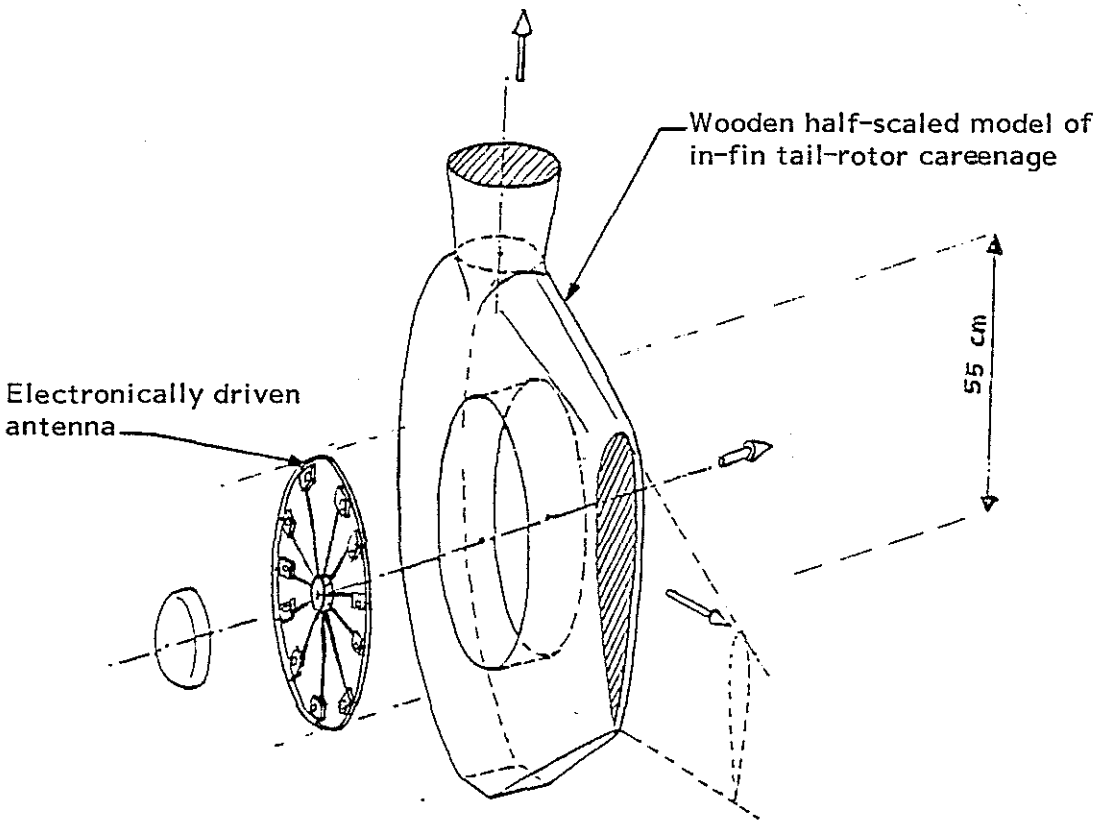

Fig. 12- Acoustic installation for diffraction measurements in the ECL anechoic room.

REFERENCES

1. D.B. Hanson — Spectrum of rotor noise caused by atmospheric turbulence. J. of the Ac. Soc. of Am. (1974) 56(1).

2. R.K. Amiet, R.W. Paterson — Noise of a model helicopter rotor due to ingestion of turbulence. J. of Sound and Vib. (1981) 85(4).

3. M.Roger, F.Fournier, P.Becker — Analyse du bruit émis par un fenestron. DRET/METRAFLU report n° 83.025 (1985).

4. R.K. Amiet — Acoustic radiation from an airfoil in a turbulent stream. J. of Sound and Vib. (1975) 41(4).

5. D.B. Hanson — Unified analysis of fan stator noise. J. of the Ac. Soc. Am. (1973)54(6).

6. J.M. Tyler, T.G. Sofrin — Axial flow compressor noise studies. SAE. Trans. (1962) 70.

7. J.M. Ville — Définition et réalisation d'un simulateur de modes tournants. ONERA Techn. note 566 (1978).

8. M.Roger, F.Fournier, P.Becker — Analyse de la diffraction des modes tournants générés par un rotor caréné. 6è Journées d'Etude Sur la Propagation Acoustique. Lyon (1986).